

Orthonormal Product Quantization Network for Scalable Face Image Retrieval

Ming Zhang, Xuefei Zhe and Hong Yan, *Fellow, IEEE*

Abstract—Recently, deep hashing with Hamming distance metric has drawn increasing attention for face image retrieval task. However, its counterpart deep quantization methods, which learn binary code representations with dictionary-related distance metrics, have seldom been explored for the task. This paper makes the first attempt to integrate product quantization into an end-to-end deep learning framework for face image retrieval. Unlike prior deep quantization methods where the codewords for quantization are learned from data, we propose a novel scheme using predefined orthonormal vectors as codewords. These predefined codewords with a fixed 90-degree angular separation aim to enhance the quantization informativeness and reduce the codewords’ redundancy. To make the most of the discriminative information, we design a tailored loss function that maximizes the identity discriminability in each quantization subspace for both the quantized and the original features. Furthermore, an entropy-based regularization term is imposed to reduce the quantization error. We conduct experiments on three commonly-used datasets under the settings of both single-domain and cross-domain retrieval. It shows that the proposed method outperforms all the compared deep hashing/quantization methods under both settings with significant superiority. The proposed codewords scheme consistently improves both regular model performance and model generalization ability, verifying the importance of codewords’ distribution for the quantization quality. Besides, our model’s better generalization ability than deep hashing models indicates that it is more suitable for scalable face image retrieval tasks.

Index Terms—Deep learning, product quantization, face image retrieval, convolutional neural networks, orthonormal codewords

I. INTRODUCTION

RAPID growth in the internet user population and the popularity of mobile devices with advanced cameras have prompted visual content sharing in various social media. Consequently, a large number of user-uploaded photos are stored every day, and a considerable portion of them are human face images, e.g., selfies and portrait photos. Due to the urgent need for image indexing and search problem, large-scale face image retrieval has drawn increasing attention over the past years. Face image retrieval aims to return the database images with the same identity as the query image. However, considering the large intra-class variance from expression, illumination, occlusion factors, and the small inter-class distance between two identities looks similar, it is still challenging to develop

an accurate and efficient system for unconstrained face image retrieval.

Towards high retrieval efficiency, one basic idea is using binary code representations to encode the data. Thus, it enables the approximate nearest neighbor (ANN) search to accelerate the query process. According to their applied distance metrics for retrieval, the works of obtaining binary code representations can be divided into two types: 1) Hamming distance-based and 2) dictionary-related distance-based. To follow the literature [1], [2], we refer to these methods, which make use of dictionary-related distance as the metric for retrieval as *quantization* models, while those works using Hamming distance as *hashing* models for the convenience of discussion. The goal of hashing is to map high dimensional real-valued data to lower dimensional binary codes in Hamming space while preserving their original similarity at the same time. Performed with the binary codes, the Hamming distance between the query and database images can be computed extremely fast by the XOR operation. Recently, deep supervised hashing was proposed to employ deep convolutional neural networks (CNNs) for end-to-end feature representations learning and hashing functions learning. And it has dramatically outperformed the traditional hashing methods on image retrieval. Existing deep supervised hashing can be roughly classified into three types according to their supervision information, i.e., pairwise labels-based [3], [4], triplet labels-based [5] or class-wise labels-based [6]–[8]. More recently, some deep hashing works were proposed for face image retrieval [9]–[11]. Basically, these works are supervised by softmax loss for classification or class-wise labels-based similarity for hashing codes compactness.

Given any pair of binary codes with length l , hashing-based methods can only generate $l + 1$ number of distinct values to depict their pairwise similarity. With such a limited number of measurements, it is hard to draw a rich similarity relation for a large-scale face image dataset with massive identities classes. Another disadvantage is, the binary codes in hashing methods are obtained by applying a sign function to the continuous features. Most prior works relax the discrete constraint to be continuous and converting it to a regularization term to solve the intractable discrete optimization. Consequently, it suffers from the inevitable loss of fine-grained features.

In parallel, product quantization (PQ) has been widely employed in the fields of computer vision and information retrieval. PQ first decomposes the feature vectors in the original space into several disjoint sub-vectors. By replacing each sub-vector with the index of the nearest codeword, the original feature in one subspace is encoded into one bit of binary

Ming Zhang and Hong Yan are with the Department of Electrical Engineering, City University of Hong Kong, Kowloon, Hong Kong SAR. Xuefei Zhe is with Tencent AI Lab, Shenzhen, China.

Email: mzhang367-c@my.cityu.edu.hk, elizhe@tencent.com, h.yan@cityu.edu.hk

code. Suppose that the binary code length $l = M \log_2 K$, where M is the number of codebooks, and K is the number of codewords in each codebook, PQ is capable of producing $\binom{K}{2}^M$ distinct values. Thus, they are more competitive to generate binary code representations of good quality. During the query stage, PQ-based methods allow the use of multiple look-up tables (LUTs) for query speed acceleration, which is only slightly more costly than hashing-based methods [12], [13]. Surprisingly, although deep hashing has drawn increasing attention for face image retrieval, deep quantization methods are rarely publicly explored for the task.

Another issue in existing deep hashing based face image retrieval is the evaluation protocol. Prior works are only limited to the single-domain retrieval. This means that the query sets used for evaluation share the same identity classes as the training sets, which have been seen to models during training. However, this evaluation protocol ignores the generalization ability of deep hashing models for unseen identities, i.e., the performance under cross-domain retrieval. As reported in [14], the hashing models that perform well under standard settings may work badly for cross-domain retrieval. Consider the real-world application where the number of newly joined identities keeps growing, it drives severe demands regarding the scalability of the retrieval system. However, the lack of cross-domain retrieval evaluation leads to prior deep hashing-based methods being unqualified for scalable face image retrieval.

The PQ technique was designed initially under unsupervised setting. For example, the codewords in PQ are iteratively updated by k -means clustering on the sub-vectors in each subspace. Recently, some deep quantization methods proposed to learn PQ with supervision, where the codewords are regarded as learnable parameters. The feature representations which are divided into several sub-vectors, are quantized by these learnable codewords depending on the vector-codewords' similarity. Typically, a softmax loss or triplet loss is constructed based on the resulting quantizations. Thereby, the learning metrics preserve the label information both in the feature representations and the learnable codewords. We refer to these deep quantization methods with the learning manner as **learning to quantization (l2q)**. However, since the codewords themselves do not contain any discriminative information in quantization process, it is possible to disentangle the discriminative visual information and codewords individually. Under this assumption, we can learn the codewords assignment of features representations even with predefined codewords. As described in subsection III-A, this is achieved by introducing one layer of parameters for quantization compositions in our method.

From another perspective, the effect of the codewords' distribution on the quantization quality is rarely explored in prior works. Intuitively, the codewords in a codebook play the role of the prototypes in each subspace. We expect these prototypes to overspread the subspace, and each of them should retain some distance from each other. Towards explicit codewords design, this paper proposes a method called Orthonormal Product Quantization Network (OPQN). Specifically, our method

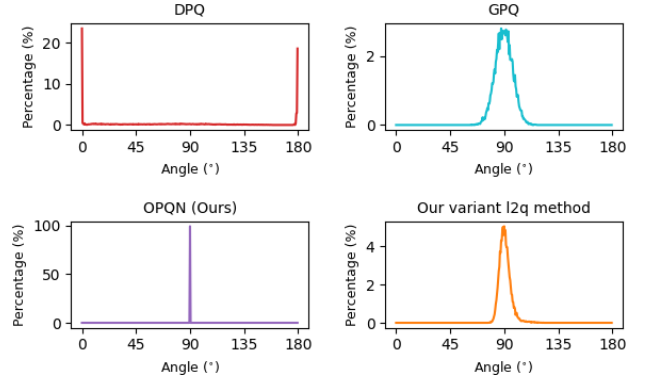


Fig. 1. Comparison of angular distribution of pairwise codewords in different deep quantization models: DPQ [1], GPQ [2], the proposed OPQN method, and the variant of our method without predefined codewords. Each angular distribution is a normalized histogram, generated by quantization from 0° to 180° , step by 0.5° .

predetermines sets of orthonormal vectors as codewords instead of learning them for use. In contrast to prior l2q works, our method belongs to **quantization to learning**. To visualize how the codewords distribute in l2q methods, we calculate the angles between each pairwise codeword of each codebook in different deep quantization models. These angle distributions over all the codewords pairs are illustrated in Fig. 1. One can observe considerable variations in the angles between learned codewords in the compared methods, whereas our method generates the angular distribution with 90° in 100%. Combined with ℓ_2 normalization on each sub-vector of feature representations, it prompts the network to learn more separable quantized features composed of predefined codewords in the hyper-sphere subspace. The main contributions of this paper are listed in three-fold as followings:

- 1) To the best of our knowledge, we make the first attempt to deploy a deep quantization model for large-scale face image retrieval. We propose a novel scheme using predefined orthonormal vectors as codewords to increase quantization informativeness and reduce codeword redundancy. The proposed scheme also enables more efficient LUTs preparation and asymmetric comparison in the retrieval phase.
- 2) To preserve the discriminability to the greatest extent, we design a tailored loss function, which maximizes the identity features' separability in each subspace. It simultaneously works on both original features and the quantized features for better quantization quality. Moreover, we propose an entropy-based regularization term to encourage the one-hot quantization compositions, which helps to improve the performance, especially under tiny bits.
- 3) Considering the limitation on the evaluation protocol in prior works, we present arguably the most comprehensive experiments serving as a supplement to the literature. We show that the proposed approach outperforms both deep quantization and deep hashing baselines for single-domain retrieval. Besides, the pre-trained model by our method generalizes the best to unseen classes for cross-

domain retrieval. The proposed codeword scheme induces consistent and noticeable improvements to both regular model performance and model generalization ability.

The rest of this paper is organized as follows. In Section II, we recall some prior works related to our approach. We present the proposed OPQN method, including codewords generation and the loss function design in Section III. In Section IV, we evaluate our method on three benchmark datasets: Face-Scrub [15], CFW-60K [16], and VGGFace2 [17] under both single-domain and cross-domain settings. In Section V, we first report the ablation study with elaboration, then discuss the model performances with respect to codebook configurations and parameter sensitivity. Finally, we conclude this paper and present the outlook for future research in Section VI.

II. RELATED WORKS

In this section, we first review some representative works on deep hashing-based face image retrieval. Then, we introduce several traditional quantization methods to make this paper be more self-contained. Finally, we introduce several state-of-the-art deep quantization methods for image retrieval.

A. Deep Supervised Hashing for Face Image Retrieval

Previous deep hashing works on face image retrieval mainly focus on network architecture design while widely adopting the softmax classification loss for supervision. Specifically, the fully connected hashing (FCH) layers transform the bottleneck features to hashing outputs in Euclidean space. And the hashing outputs are usually supervised by a softmax classifier. Generally, a quantization loss is additionally imposed to relax the discrete binary constraint to be continuous and reduce the quantization error. In Discriminative Deep Hashing (DDH) [9], researchers first proposed to train deep CNNs with a divide-and-encode module to obtain the compact binary codes for face image retrieval. Following DDH, Discriminative Deep Quantization Hashing (DDQH) [10] found that the retrieval performance can be further enhanced by inserting a batch normalization layer between the FCH layer and the Tanh activation function. Deep Clustering and Block Hashing (DCBH) [18] introduced a block hashing layer to decrease hashing codes redundancy and the number of parameters. More recently, some works were proposed to utilize the label information with other supervisions. In Deep Discrete Attention Guided Hashing (DAGH) [19], researchers imposed a discrete identity loss to effectively compact intra-identity variations. Inspired by the class-wise labels-based similarity, Deep Center-based Dual-constrained Hashing (DCDH) [11] proposed a center-based framework to learn hashing functions and class centers end-to-end jointly. With the proposed dual constraint on class centers, DCDH showed state-of-the-art results on face image retrieval.

B. Traditional quantization techniques

The most classical quantization technique is Vector Quantization (VQ), which quantizes the feature space by maintaining one codebook. Suppose that the codebook consists of K

codewords, VQ divides the feature space into K clusters using unsupervised clustering methods, e.g., k -means. Thus, each feature vector can be encoded by $\log_2 K$ bits. And the LUT, which stores the pre-computed distance matrix between every two clusters, has $\mathcal{O}(K^2)$ entries. However, the increase in VQ's bit length leads to exponential growth in the number of clusters K , while the number of entries in LUT grows quadratically with K , making it impractical to use a large value of K . Consequently, it becomes the bottleneck to restrict the performance of VQ. Fortunately, PQ [12] is proposed to overcome the model capacity problem of VQ. PQ decomposes a feature vector $x_i \in \mathbb{R}^{Md}$ into M disjoint sub-vectors with dimension d , i.e. $x_i = [x_{i1}, x_{i2}, \dots, x_{iM}]$. The sub-vector x_{im} is related to the m -th subspace which is quantized by the corresponding codebook $C_m = [C_{m1}, C_{m2}, \dots, C_{mK}] \in \mathbb{R}^{d \times K}$ composed of K codewords. One can see that PQ can achieve an exponential number of K^M combinations of codewords to represent a feature vector by M codebooks. Therefore, it outperforms VQ with more expressive power for quantization. Later on, a variety of optimized PQ methods were developed, such as AQ [20] and CQ [21], which achieve more accurate space decomposition and codeword learning.

C. Deep Quantization Methods for General Image Retrieval

Recently, deep quantization methods have emerged as an effective solution for image retrieval tasks, integrating quantization into deep CNNs for simultaneous feature learning and codeword learning. In [13], Deep Quantization Network (DQN) introduced a combined loss consisting of similarity-preserving loss and product quantization loss. Deep Triplet Quantization (DTQ) [22] proposed to use CQ [21] and triplet sampling for quantization and feature learning, respectively. Deep Product Quantization (DPQ) [1] was the first work based on learning PQ representations end-to-end with supervision. It learns both soft and hard quantizations for a more accurate asymmetric search. And a straight-through (ST) estimator is applied to enable back-propagation (BP) on the $\text{argmax}(\cdot)$ function. Alternatively, Product Quantization Network (PQN) [23] introduced a soft PQ layer, which directly determines the codeword assignment from the cosine similarity between features and codewords. Specifically, both x_{im} and C_{mk} are ℓ_2 normalized with unit length so that their similarity can be reflected from their inner product directly. The soft quantization s_{im} of x_{im} in PQN is shown as:

$$s_{im} = \sum_{k=1}^K \frac{e^{\alpha \langle x_{im}, C_{mk} \rangle}}{\sum_{j=1}^K e^{\alpha \langle x_{im}, C_{mj} \rangle}} C_{mk} = \sum_{k=1}^K u_{mk} * C_{mk} \quad (1)$$

where α is a scaling factor. Note that when $\alpha \rightarrow +\infty$, $u_{mk} \rightarrow \mathbb{1}(k = k_*)$, which is a one-hot encoding vector with one on the k_* -th entry but zeros elsewhere. Here, $k_* = \text{argmax}_k x_{im}^T C_{mk}$, represents the index of the most similar codewords for hard quantization. PQN avoids the infeasible derivative caused by $\text{argmax}(\cdot)$, and it allows the network to be optimized by the standard gradient descent algorithm.

Existing deep quantization methods all target general image retrieval, and they may not be competitive for face image retrieval tasks. For example, PQN proposed an asymmetric

triplet loss as the similarity metric. However, it requires a complex hard sample mining strategy during training, and the computational cost is prohibitive when using a large number of triplet samples. DPQ applied a joint central loss based on the classical softmax loss. However, it has been shown that angular margin-based methods are superior in acquiring discriminative power for classification. Another problem is that in terms of better quantization performance, what kind of codewords in deep quantization models are preferred? As shown in Fig. 1, the codewords in previous **I2q** works have significant variations in angle distribution. Thus, they are inferior concerning quantization informativeness and codeword diversity.

III. ORTHONORMAL PRODUCT QUANTIZATION

Unlike the previous deep quantization works where the codewords are learned either in an unsupervised or supervised manner from data, this work alternatively uses sets of predefined orthonormal codewords for quantization. Besides, we design a subspace-wise joint classification loss, providing sufficient discriminating power for PQ-based similarity search. The overview of the proposed method is illustrated in Fig. 2.

The notations used in this paper are introduced as follows. We denote a dataset with N face images as $\{I_i\}_{i=1}^N$, and the corresponding label vector as $y \in \mathbb{R}^N$. For an input image I_i , $x_i \in \mathbb{R}^D$ is the bottleneck features as shown in Figure 2 produced by the backbone network $f(\Theta)$, where Θ are the backbone network parameters. x_i is divided into M disjoint sub-vectors with dimension $d = D/M$, i.e., $x_i = [x_{i1}, x_{i2}, \dots, x_{iM}]$ where $x_{im} \in \mathbb{R}^d$. Assume the codebooks $C = [C_1, C_2, \dots, C_M] \in \mathbb{R}^{M \times d \times K}$ and each codebook consists of K codewords, i.e., $C_m = [C_{m1}, C_{m2}, \dots, C_{mK}] \in \mathbb{R}^{d \times K}$. We denote the soft quantization and hard quantization of x_{im} as s_{im} and h_{im} , respectively. Concretely, $h_{im} = C_{mk_*}$, is the approximation of x_{im} by the codeword with index k_* in m -th codebook. Thus, the soft quantization and hard quantization of I_i can be represented as $s_i = \{s_{im}\}_{m=1}^M$ and $h_i = \{h_{im}\}_{m=1}^M$, respectively.

A. Soft quantization via feature-probability disentanglement

The soft quantization shown in Eq. (1) implicitly encodes the similarity between sub-vectors and codewords. Consequently, how each codeword constitutes s_{im} and how far the distance between s_{im} and C_{mk_*} are both obscure to observe. Besides, as the scaling factor cannot be set to positive infinity, there is always a gap between s_{im} and h_{im} . Instead, our method learns the codewords assignment explicitly via an intermediate fully connected layer. Note that since the codewords are now predefined in our approach, it offsets the number of parameters in the intermediate layer. Thus, the total number of learnable parameters does not grow compared to prior works such as PQN [23] and GPQ [2]. Inspired by DPQ [1], a linear transformation layer is built on top of each sub-vector x_{im} individually. And the parameter matrices in all the linear transform layers are denoted as $F = [F_1, F_2, \dots, F_M] \in \mathbb{R}^{M \times d \times K}$. For simplicity, we omit the biases in each layer. With a softmax function appending

the layer outputs, the probability of assigning the codeword C_{mk} to the subvector x_{im} can be formulated as:

$$p_{im,k} = \frac{e^{x_{im}^T F_{mk}}}{\sum_{j=1}^K e^{x_{im}^T F_{mj}}} \quad (2)$$

where F_{mj} is the j -th column of the parameter matrix F_m . The K probabilities are concatenated to the vector: $p_{im} = [p_{im,1}, p_{im,2}, \dots, p_{im,K}] \in \mathbb{R}^K$. The soft quantization s_{im} of x_{im} in the proposed method is represented as:

$$s_{im} = \sum_{k=1}^K p_{im,k} * C_{mk} \quad (3)$$

Eq. (3) means each soft quantization s_{im} is the convex combination of $\{C_{mk}\}$ with softmax coefficients p_{im} . Based on this, one can naturally derive the hard quantization as $h_{im} = C_{mk_*}$. Here, k_* is the index of the codeword with the largest value in p_{im}^i , formulated as:

$$k_* = \underset{k}{\operatorname{argmax}} p_{im,k} \quad \text{s.t.} \quad k = 1, 2, \dots, K \quad (4)$$

Note that our method does not compute the hard quantization in the training process, which avoids handling the derivative problem of $\operatorname{argmax}(\cdot)$. Eq. (4) only serves to encode database items during testing, which will be detailed in subsection III-F.

B. Orthonormal codewords generation

The above soft quantization method disentangles the sub-vectors and codewords by learning a linear transform matrix to represent the quantization composition. Thus, it provides the feasibility of using predefined codewords for quantization. Assume there is a codebook C_m , each column of which is a codeword. We know, for any pair of codewords C_{mi} and C_{mj} : $0 \leq \angle(C_{mi}, C_{mj}) \leq \pi$. The basic idea of codeword design is to improve the quantization informativeness as well as reducing the codewords redundancy. We expect each codeword to keep a separable angle from each other and the variance of angles, $\angle(C_{mi}, C_{mj})$ to be as small as possible. To eliminate the side effect caused by the magnitude in C_{mi} , C_{mi} should be normalized with unit length. In terms of these two aspects, we decide to apply the orthonormal vectors as codewords, which possess the following desirable characteristics:

- $\|C_{mk}\| = 1$
- $C_m^T C_m = I_K$

We can see that the orthonormal vectors are of unit norm naturally. Meanwhile, every two different orthonormal vectors keep a $\pi/2$ angular separation from each other.

There are multiple choices to generate a set of orthonormal vectors. For example, one can simply run Singular Value Decomposition (SVD) on a random matrix and return the columns of the left-singular vectors as codewords. However, a better solution is to use deterministic orthonormal vectors that excludes the randomness biases caused by codewords themselves. Thereby, we utilize the cosine basis of Discrete Cosine Transform (DCT) [24], specifically, DCT-II algorithm. Suppose the dimension of sub-vectors, as well as codewords,

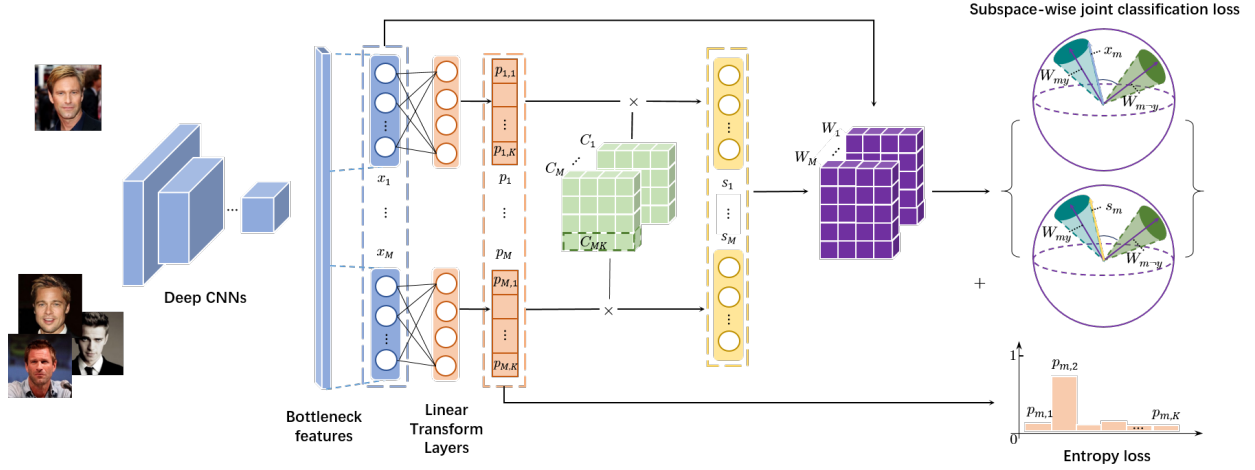


Fig. 2. The overview of the proposed OPQN method. Here, x_m represents the sub-vector from the bottleneck features. Each sub-vector is projected by a linear transform layer followed by softmax operation to produce the probability vector p_m . Then, the soft quantization s_m is represented as a convex combination between p_m and orthonormal codewords C_m . By the weight matrix W_m , the classification loss jointly maximizes the discriminability of x_m and s_m in each subspace. Besides, an entropy-based regularization term is applied to p_m to encourage one-hot encoding assignment.

are d , the basis matrix $A \in \mathbb{R}^{d \times d}$ in DCT-II transform can be obtained as:

$$A_{ij} = \cos\left[\frac{j\pi}{d}\left(i + \frac{1}{2}\right)\right] \quad s.t. \quad i, j = 1, 2, \dots, d \quad (5)$$

By several processing steps on A , we could obtain an orthogonal matrix A^\dagger , whose first K column vectors are the desired codewords in one codebook. Recall that the orthonormal vectors multiplied by an orthogonal matrix are still orthonormal vectors. Thus, we iteratively multiply the previous codebook by A^\dagger to get the new codebook, which guarantees the diversity between different sets of codebooks while still retaining the orthonormality of each codebook. The whole procedure of orthonormal codewords generation based on cosine basis is summarized in Algorithm 1. One thing noted that our method requires the number of codewords is no more than the dimension of sub-vectors. For a network with bottleneck 2048-dimensional features, it is able to generate binary codes with code length up to 64-bit ($8 \log_2 256$), which is sufficient to cover most cases.

Algorithm 1 Deterministic orthonormal codewords generation

Input: Dimension of feature representations D , number of codebooks M , number of codewords per codebook K , dimension of sub-features d , where $d = D/M$ and $K \leq d$

Output: Codebooks $C \in \mathbb{R}^{M \times d \times K}$

- 1: Compute the cosine basis matrix A according to Eq. (5)
 - 2: $A[:, 0] \leftarrow A[:, 0]/\sqrt{2}$
 - 3: $A^\dagger \leftarrow \sqrt{2}A/\sqrt{d}$
 - 4: $C_1 = A^\dagger[:, :K]$
 - 5: **for** $m = 2 : M + 1$ **do**
 - 6: $C_m = A^\dagger * C_{m-1}$
 - 7: **end for**
-

C. Subspace-wise joint classification loss

By substituting the codewords in Eq. (3) with the predefined orthonormal codewords generated in Algorithm 1, we can

obtain the soft quantization of feature vectors in each subspace. These quantized features will be fed into our carefully designed objective function supervised with label information for discriminative face image retrieval. Nevertheless, it is natural that the bottleneck features directly limit the quantization performance. The well-learned original features should benefit the embedding of identity-specific clues in quantized features. Therefore, we propose to preserve the feature discriminability both in the original features and soft quantized features.

From another view, since the original features and its quantized version have fallen into several disjoint subspaces in PQ-based methods, the associated full identity information also breaks into different partitions. Towards better classification, we expect intra-identity features and the soft quantizations to be separable from those belonging to other identities in each subspace. Thus, one solution is learning a set of subspace-wise classifiers individually for each segment of x_{im} and s_{im} .

We denote a fully connected layer containing a set of weight matrices as $W = [W_1, W_2, \dots, W_M] \in \mathbb{R}^{M \times d \times C}$, where C is the number of identity classes in the datasets. W_{mc} represents the c -th column vector of W_m in the m -th subspace. Following the popularity of ℓ_2 normalization on weights in deep face recognition, we normalize W_{mc} : $W_{mc} \leftarrow W_{mc}/\|W_{mc}\|_2$. Correspondingly, x_{im} is also ℓ_2 normalized: $x_{im} \leftarrow x_{im}/\|x_{im}\|_2$. Thus, it facilitates the cosine similarity between x_{im} and W_{mc} directly implied from their inner product. Specifically, $\cos \theta_{y_i, x_{im}} = x_{im}^T W_{m y_i}$, where $\theta_{y_i, x_{im}}$ represents the angle between x_{im} with label y_i and its corresponding weight vector $W_{m y_i}$. Inspired by the popular and effective line of angular margin-based deep face recognition [25], [26], we add a cosine margin u between the $\cos \theta_{y_i, x_{im}}$ and $\cos \theta_{y_{-i}, x_{im}}$. The introduced margin helps to enhance the intra-identity compactness and inter-class discriminability of the original features in each subspace. By formulating the angular margin into the softmax classification loss and summing up the loss terms coming from all the M segments, we obtain the loss function concerning x and W

shown as:

$$L_x = \sum_{i=1}^N \sum_{m=1}^M -\log \frac{e^{r(\cos \theta_{y_i, x_{im}} - u)}}{e^{r(\cos \theta_{y_i, x_{im}} - u)} + \sum_{j \neq y_i} e^{r \cos \theta_{j, x_{im}}} \quad (6)$$

where r is a scaling factor to re-scale the normalized sub-features. Likewise, we also ℓ_2 normalize the s_{im} to remove the radius variation. Then, the cosine distance between s_{im} and W_m is indicated by their multiplication, and the angle between s_{im} and $W_{m y_i}$ is denoted as $\theta_{y_i, s_{im}}$. Similarly, the angular margin-based loss function w.r.t. s and W is formulated as:

$$L_s = \sum_{i=1}^N \sum_{m=1}^M -\log \frac{e^{r(\cos \theta_{y_i, s_{im}} - u)}}{e^{r(\cos \theta_{y_i, s_{im}} - u)} + \sum_{j \neq y_i} e^{r \cos \theta_{j, s_{im}}} \quad (7)$$

It is noteworthy that the values of margin u and scaling factor r in Eq. (7) are the same as in Eq. (6) to encourage the consistency between x_{im} and s_{im} . Combine Eq. (6) and Eq. (7), the joint similarity-preserving loss is represented as:

$$\min_{\Theta, F, W} L_{clf} = \frac{1}{2MN} (L_x + L_s) \quad (8)$$

The above Eq. (8) targets subspace-wise intra-identity variance minimization and inter-identity variance maximization for both original features and the quantized features.

D. Entropy minimization for one-hot codewords assignment

The above joint classification loss with regularization utilizes the soft quantization s_{im} without considering the hard quantization h_{im} in training. However, we would like to reduce the discrepancy between s_{im} and its corresponding original version h_{im} . In other words, the probability vector p_{im} which takes the role of codewords assignment are supposed to be close to one-hot encoding. Therefore, we propose an entropy-based regularization term to force the learned sub-feature to move towards a single codeword while pushing it apart from other codewords. The entropy-based loss is formulated as following:

$$L_{ent} = -\frac{1}{MN} \sum_{i=1}^N \sum_{m=1}^M \sum_{k=1}^K p_{im,k} \log p_{im,k} \quad (9)$$

As we have known, $p_{im,k} \log p_{im,k}$ gets the minimum value 0 if and only if $p_{im,k} = 0$ or $p_{im,k} = 1$. Under the constraint of $\sum_k p_{im,k} = 1$, the proposed entropy loss tends to shape the p_{im} 's distribution into the pattern with single peak at one index while small values elsewhere. By adding up the loss terms from all the M probability vectors, it accomplishes the discrepancy reduction between s_i and h_i for more precise quantization. By integrating L_{clf} and L_{ent} , we get the finalized loss function of the proposed method:

$$L = L_{clf} + \lambda L_{ent} \quad (10)$$

where λ is a balance weight of the entropy loss.

E. Learning and optimization

The proposed orthogonal PQ network contains three parts of learnable parameters: backbone network parameters Θ , the linear transform layer parameters F and the classification weight W . We adopt the mini-batch strategy and stochastic gradient descent (SGD) in training and all the parameters can be learned by BP. Denote x_{im}^T multiplied by F_m shown in Eq. (2) as $g_m = [g_{m1}, g_{m2}, \dots, g_{mK}]$. The gradients of p_{im} w.r.t g_m can be computed as follows:

$$\frac{\partial p_{im,k}}{\partial g_{mk}} = p_{im,k}(1 - p_{im,k}); \quad \frac{\partial p_{im,k}}{\partial g_{mj}(j \neq k)} = -p_{im,k} p_{im,j} \quad (11)$$

Thus, we can derive the gradient of the soft quantization s_{im} w.r.t. g_{mk} by BP:

$$\frac{\partial s_{im}}{\partial g_{mk}} = \left[\frac{\partial s_{im}}{\partial p_{im}} \right]^T \frac{\partial p_{im}}{\partial g_{mk}} = p_{im,k} (C_{mk} - s_{im}) \quad (12)$$

Similarly, since $\partial L_{ent} / \partial p_{im} = -(1 + \log p_{im})$, we obtain the derivatives of L_{ent} w.r.t. g_{mk} using Eq. (11) as:

$$\frac{\partial L_{ent}}{\partial g_{mk}} = p_{im,k} \left(\sum_{j=1}^K p_{im,j} \log p_{im,j} \right) - p_{im,k} \log p_{im,k} \quad (13)$$

Combining Eq. (12) and Eq. (13), then apply BP, the derivative of L regarding F_{mk} is shown as:

$$\frac{\partial L}{\partial F_{mk}} = \left[\frac{1}{2} \left(\frac{\partial L_s}{\partial s_{im}} \right)^T \frac{\partial s_{im}}{\partial g_{mk}} + \lambda \frac{\partial L_{ent}}{\partial g_{mk}} \right] x_{im} \quad (14)$$

Likewise, the derivative of L regarding W is calculated by:

$$\frac{\partial L}{\partial W_{mk}} = \frac{1}{2} \left(\frac{\partial L_x}{\partial W_{mk}} + \frac{\partial L_s}{\partial W_{mk}} \right) \quad (15)$$

Finally, the derivative of L w.r.t. x_{im} is:

$$\frac{\partial L}{\partial x_{im}} = \frac{1}{2} \frac{\partial L_x}{\partial x_{im}} + \frac{1}{2} \left(\frac{\partial L_s}{\partial g_{mk}} + \lambda \frac{\partial L_{ent}}{\partial g_{mk}} \right) F_{mk} \quad (16)$$

F. Asymmetric distance comparison for retrieval

Once the training procedure is completed, we can build an image retrieval system. The query and database items in the searching phase are handled with different processing procedures. Given a query image q , we propagate it through the model until the linear transform layers. The outputs are followed by the softmax function as in Eq. (2) to obtain the probability vector p_{qm} of each subvector x_{qm} . While for each database image I_i , we repeat the same procedure as the query image. Additionally, each database image is associated with its hard quantization via the index of the largest value in p_{im} . Suppose a matrix $B \in \mathbb{R}^{N \times M}$, where each element b_{im} stores the index k_* of codewords in Eq. (4).

The asymmetric quantization distance (AQD) [12] enables using soft quantizations s_q to represent a query but hard quantizations h_i to encode database images. It takes the advantages of both memory footprint reduction and retrieval speed acceleration. Here, we also use AQD as the similarity

metric, which computes the Euclidean distance between a query q and a database image I_i as follow:

$$AQD(q, I_i) = \sum_{m=1}^M \|s_{qm} - h_{im}\|_2^2 = \sum_{m=1}^M \|C_m p_{qm} - C_{mb_{im}}\|_2^2 \quad (17)$$

Note the orthogonality of C_m . By expanding the most right-hand side of Eq. (17) and eliminating the constant and the term irrelevant to $C_{mb_{im}}$, we can derive the following equation:

$$\begin{aligned} \operatorname{argmin}_i AQD(q, I_i) &= \operatorname{argmin}_i \sum_{m=1}^M -2p_{qm}^T C_m^T C_{mb_{im}} \\ &= \operatorname{argmax}_i \sum_{m=1}^M p_{qm, b_{im}} \end{aligned} \quad (18)$$

From Eq. (18), $\operatorname{argmin}_i AQD(q, I_i)$ depends on $\{p_{qm}\}_{m=1}^M$ and $\{b_{im}\}_{m=1}^M$. It indicates the quantization similarity comparison between the query and any database item can be realized efficiently by indexing p_{qm} with some LUTs. Specifically, we can build M LUTs denoted as $\{LUT_m\}$, w.r.t., M probability vectors $\{p_q\}$, respectively, where $LUT_m[i] = b_{im}$. Since the matrix B can be pre-computed, it only takes several addition calculations in the searching process. Compared with other PQ methods, our proposed OPQN has dual advantages. Firstly, unlike DQN [13] and DPQ [1], our method does not require explicit online soft quantization reconstruction or Euclidean distance calculation between the soft quantization and each codeword. Therefore, it is more scalable and time-saving to handle the query which arrives on-the-fly. Secondly, the codebooks in our method are data-independent and predefined. It allows models to use the same codebook for different datasets, which contributes to lowering the system's storage cost. The whole training and retrieval procedures of OPQN are summarized in Algorithm 2.

IV. EXPERIMENTS AND RESULTS

A. Datasets and evaluation metrics

To demonstrate the performance of the proposed OPQN, we conduct experiments on three commonly-used publicly available datasets, including FaceScrub [15], CFW-60K [16], and VGGFace2 [17]. The details of each dataset with the corresponding protocol are summarized as follows:

1) *FaceScrub*: FaceScrub [15] contains 106,863 face images of 530 celebrities with about 200 images per identity. We use the same training-test split as in [9], [10]: five images per identity are selected for testing, and the remaining images are used for training. All the face images have been cropped and resized to 32×32 .

2) *CFW-60K*: CFW-60K [16] is a dataset containing 60,000 images of 500 identities. Following the same configuration as in [11], we use the official test split in CFW-60K, which has 10 images per identity and a total of 5000 images for testing. Among the other images, a total number of 55,000 images with category labels are used for training. The training-testing split was used as database images and queries, respectively, under both single-domain and cross-domain retrieval tasks.

Algorithm 2 OPQN Training and Top- k Retrieval Procedure

Training stage

Input: Training set $\{I_i\}_{i=1}^N$ with labels y , the network $f(\cdot)$, the dimension of codebooks: $M \times d \times K$;

Initialization: Backbone network parameters Θ , linear transform layer F , classification weight matrix W ;

- 1: Generate orthonormal codewords by Algorithm 1;
- 2: **Repeat**
- 3: Randomly sample a mini-batch data from training set;
- 4: Feed forward the mini-batch images through the model and compute $x_i = f(\Theta; I_i)$ for each image;
- 5: Calculate the object function L according to Eq. (10);
- 6: Compute the derivatives of L w.r.t. W , F and x_{im} according to Eq. (15), Eq. (14) and Eq. (16), respectively;
- 7: Back propagate the gradients to the backbone network, then update the parameters W , F and Θ ;
- 8: **Until** Convergence

Retrieval stage

Input: Database images $DB = \{db_i\}_{i=1}^{|DB|}$, query set images $Q = \{q_i\}_{i=1}^{|Q|}$, the trained model;

Output: Top k instances in DB for each q_i ;

- 1: Forward pass DB through the model in advance, and pre-compute the indices matrix B according to Eq. (2) and Eq. (4);
 - 2: LUTs construction for DB based on matrix B ;
 - 3: **for** i **in** $1, 2, \dots, |Q|$:
 - 4: Forward pass q_i through the model and compute $p_{q_i, m}$ by Eq. (2);
 - 5: Compute similarity between q_i to each database image by Eq. (18) using LUTs, and sort the result in descending order;
 - 6: Return top k instances in DB ;
 - 7: **end**
-

3) *VGGFace2*: The official VGGFace2 [17] dataset contains 3.31 million images of 9,131 identities, split into 8,631 identities for training and 500 identities for testing. The identities in the training testing split are disjoint. We choose 2,781 identities whose number of images are around 300 from the official training set. We further split 50 images per identity from those 2,781 classes for testing, while the rest images are all used for training. Under the single-domain retrieval protocol, the training set is employed as the database while the test set is used as queries. In the cross-domain retrieval protocol, we take all the identities in the official test set. 50 images per identity are split as queries, while the rest are used as a database. All the images in VGGFace2 are cropped and aligned following the instructions of MTCNN [27]. Each image is resized to 112×112 .

Three kinds of standard evaluation metrics are applied to evaluate the retrieval quality: mean average precision (mAP), precision w.r.t. top T returned images ($P@T$), and precision-recall (PR) curve.

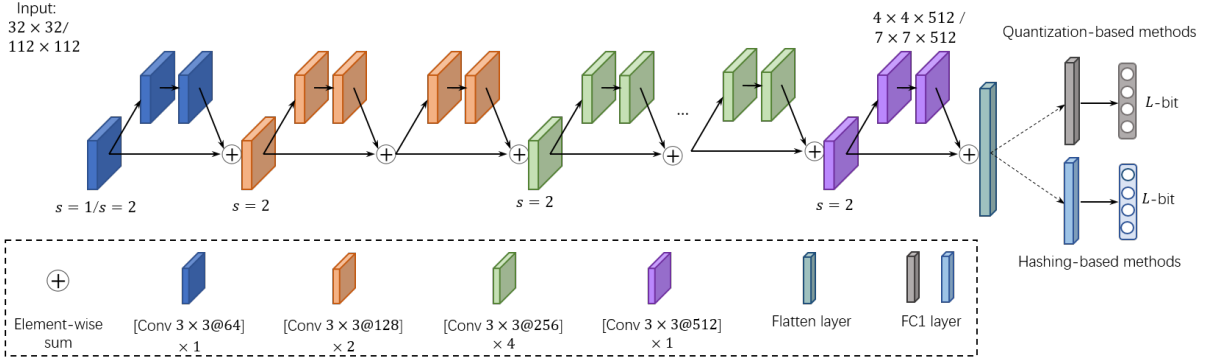


Fig. 3. The applied network with ResNet20 architecture. ‘[Conv3 × 3@ ϕ] $\times\psi$ ’ represents a number of stacked ψ residual blocks with a kernel size of 3 × 3 that output ϕ -channel feature maps. The first convolutional layer of the first block applies unit stride or stride of 2 depending on the input size, as separated by ‘/’, respectively, while the first layers in other blocks are all performed with a stride of 2 for down-sampling.

B. Experiment settings

We compare the proposed OPQN method with a series of binary hashing-based and PQ-based methods. Specifically, we conduct experiments on a set of deep hashing methods, including DDQH [10], DCWH [6], DPAH [28], and DCDH [11], where DDQH and DCDH are originally developed for face image retrieval, while others aim at general image retrieval tasks. For the PQ-based method, we test DPQ [1] and GPQ [2] for comparison. Note that all the compared PQ methods are initially designed for general image retrieval. To ensure a fair comparison, we unify the backbone network for all the compared binary hashing methods and PQ-based methods. Thus, the difference of the applied networks between binary hashing methods and PQ-based methods only exists in the last few layers, which necessarily distinguishes the approach from each other. Without loss of generality, the employed backbone network is based on the ResNet20 [29] architecture, shown in Fig. 3. Similar architectures have also been used in some prior deep face recognition works [26], [30]. As illustrated in Fig. 3, for quantization-based methods, the outputs of the last convolutional layer are flattened and projected into the FC1 layer to generate the bottleneck features shown in Fig. 2. In contrast, for hashing-based methods, the flattened convolutional layer’s outputs are first transformed into 512-dimensional by the FC1 layer, followed by a FCH layer to produce hashing outputs with expected code length. Note that we apply dropout [31] to the flatten layer, and batch normalization [32] is used after each fully connected layer in two branches of methods.

C. Implementation details

We evaluate the performance of the proposed method under various code lengths ranging from 16 bits to 64 bits. During training, our method uses a mini-batch SGD algorithm for optimization with momentum of 0.9 and weight decay of 5e-4. For small datasets, i.e., FaceScrub and CFW-60K, the initial learning rate is set to 0.1 and decayed by 0.5 every 35 epochs, while in VGGFace2 dataset, we set the initial learning rate to 0.01 and decay it by 0.5 every 20 epochs. The batch size is fixed to 256 for all the datasets, and we train the whole

network for 200 epochs. According to cross-validation, the parameter setting in our method is: the scaling factor $r = 40$, the margin $u = 0.4$, and the balance weight $\lambda = 0.1$. We apply the same data augmentation process to all the methods during training: the images are first enlarged to about 1.1 times the original input size. Then, they are randomly cropped to the original size with random horizontal flipping. We run the experiments of compared methods if the codes are available from the original authors. Otherwise, we carefully implement the methods by ourselves. All the experiments are run on two Nvidia RTX-2080 GPU cards with PyTorch.

D. Group 1: Single-domain retrieval

We first conduct experiments on the proposed OPQN on FaceScrub and CFW-60K datasets, following the standard single-domain retrieval protocol in prior works. We evaluate the binary codes under 16 bits, 24 bits, 36 bits, and 48 bits, and the number of codebooks M are empirically set to 2, 4, 6, and 8, respectively. Thus, the number of codewords in each codebook K are 256, 64, 64, and 64 accordingly. Note that the bottleneck features with dimension D should fulfill the conditions that $D/M \leq K$ and $D|M$. For simplicity, we fix D to 512 for all the cases except 36 bits. Under 36-bit code, we tweak D to 516 to be divisible by the number of codebooks, i.e., 6. The compared PQ-based methods adopt the same codebook and codeword settings as in our method.

The MAP results on FaceScrub and CFW-60K datasets under four kinds of code length are summarized in Table I. For the convenience of comparison, we denote the results of DDQH and DCDH methods in the original paper as DDQH* and DCDH*, which apply different backbone networks from ours. Here, we also present the result of the variant of our method, denoted by OPQN-l2q. Specifically, it employs the same learning metric as ours while the codewords are learned instead of predefined, as in DPQ and GPQ. From Table I, we can see that the proposed OPQN outperforms all the compared baselines over the entire code lengths ranging from 16 to 48 bits. Concretely, compared to the state-of-the-art deep hashing method DCDH, the proposed OPQN achieves performance improvements of 3.75% and 2.14% on average for FaceScrub and CFW-60K, respectively. The superiority of our method

TABLE I
MAP RESULTS ON FACESCRUB AND CFW-60K UNDER THE SINGLE-DOMAIN SETTING

Method	FaceScrub				CFW-60K			
	16-bit	24-bit	36-bit	48-bit	16-bit	24-bit	36-bit	48-bit
DDQH*	-	0.4482	0.5071	0.5191	-	-	-	-
DDQH	0.8393	0.8561	0.8714	0.8828	0.7832	0.7880	0.8069	0.8222
DCWH	0.8352	0.8445	0.8562	0.8872	0.7014	0.7251	0.7480	0.7839
DPAH	0.8398	0.8859	0.9006	0.9041	0.7602	0.8266	0.8399	0.8454
DCDH*	-	0.7779	0.8347	0.8464	-	0.8168	0.8356	0.8548
DCDH	0.8496	0.8718	0.8953	0.9143	0.8055	0.8608	0.8669	0.8716
DPQ	0.3870	0.8405	0.9043	0.9071	0.3043	0.5761	0.7037	0.7055
GPQ	0.6338	0.8036	0.8593	0.8699	0.6402	0.4931	0.6146	0.7190
OPQN (Ours)	0.9032	0.9154	0.9270	0.9385	0.8547	0.8637	0.8826	0.8940
OPQN-l2q	0.6273	0.8971	0.9162	0.9254	0.5278	0.8351	0.8725	0.8780

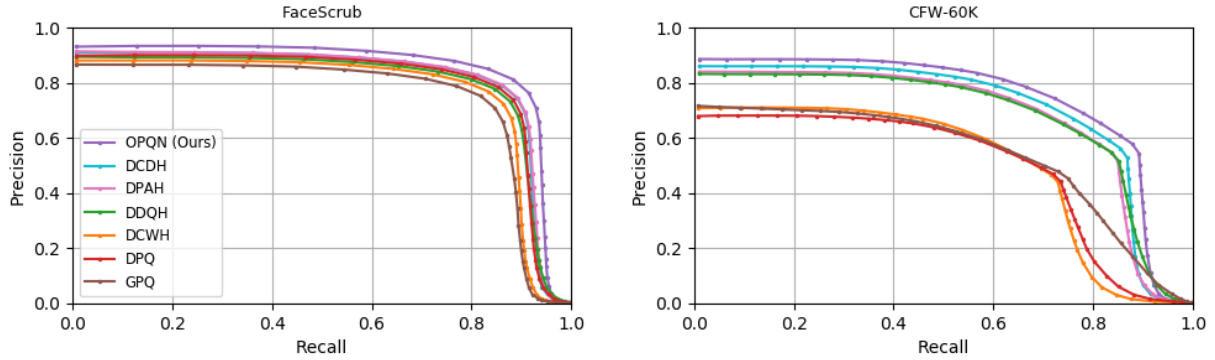


Fig. 4. Comparison of PR-curve performance under 48-bit codes on FaceScrub and CFW-60K datasets.

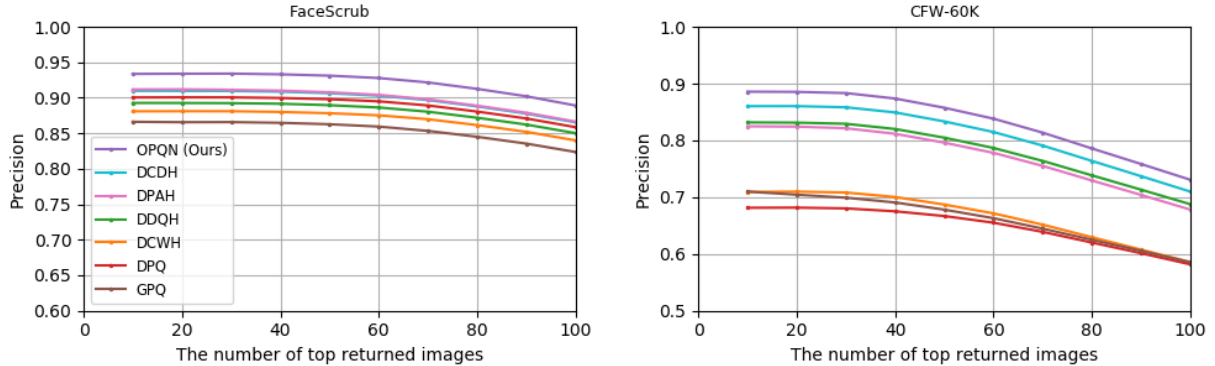


Fig. 5. Performances w.r.t. different P@T results under 48-bit codes on FaceScrub and CFW-60K datasets.

is more prominent under short code lengths than longer bits. For example, under 16-bit codes, our method outperforms the second place DCDH by a margin of 5.36% and 4.92% on two datasets, respectively. Since DCDH uses more complex regularization terms than ours, it proves the feasibility of quantization-based face image retrieval.

However, one can observe that other deep quantization models, i.e., DPQ and GPQ, do not perform as well as deep hashing-based methods. Particularly, the performances of DPQ and GPQ are poor under 16-bit codes. The reason may be that their applied learning metrics are insufficient to extract discriminative features. The cases become more challenging for PQ-based methods since the complete visual information

attached to the feature vector is divided into several subspaces. However, our method of maximizing the discriminability of both soft representations and sub-vectors in each subspace is competitive to handle this challenge. It is worth noting that the variant OPQN-l2q performs inferior to the original OPQN under various compared code lengths. From 24 to 48 bits codes, its performances are 1.31% and 1.66% lower than ours on average on two datasets, respectively, while for 16-bit codes, its performances substantially deteriorate, namely 27.59% and 32.69% lower than the proposed OPQN. The results strongly support the effectiveness of the proposed orthonormal scheme.

The performances on the PR-curve under 48-bit codes are

shown in Fig. 4. We can see that the PR curves of our proposed OPQN almost always span outermost from the top-left to the bottom-right corner of the whole figures for two datasets. This means that our method can maintain a higher precision with the increase in the recall score. Since face image retrieval system users generally only look through the top ranking images, it is also necessary to evaluate the retrieval accuracy in terms of a different number of top returned images. Therefore, we plot the precision curves w.r.t. the number of top returned images ranging from 10 to 100 in Fig. 5. It is clear that our method consistently achieves the best precision compared to other methods, which verifies its capability of providing superior retrieval results over a moderate quantity of returns.

TABLE II
MAP RESULTS ON VGGFACE2 UNDER THE SINGLE-DOMAIN SETTING

Method	VGGFace2			
	24-bit	36-bit	48-bit	64-bit
DDQH	0.8119	0.9014	0.9167	0.9289
DCWH	0.3423	0.5224	0.6458	0.7259
DPAH	0.8159	0.8715	0.8897	0.9042
DCDH	0.8752	0.9095	0.9181	0.9232
DPQ	0.7105	0.7703	0.8435	0.8681
GPQ	0.6790	0.7041	0.7286	-
OPQN (Ours)	0.8986	0.9508	0.9504	0.9529
OPQN-l2q	0.7600	0.8575	0.9127	0.9059

We further conduct experiments on the employed VGGFace2 dataset. We evaluate four kinds of code length i.e., 24-bit, 36-bit, 48-bit, and 64-bit. In our method, the number of codebooks are set to 3, 4, 6, and 8, respectively. Accordingly, the number of codewords in each codebook is 256 in the cases of 24-bit, 48-bit and 64-bit, while 512 for the 36-bit case. Recall the requirements on the bottleneck features’ dimension D in our method. Here we adopt the setting of $D = MK$. For a fair comparison, we evaluate the DPQ [1] method with the same configuration of D , M , K as our method, while for GPQ [2] method, we find it can only perform well with a large value of K in our case. Thus, we fix K to 4096 (2^{12}), and M to 2, 3, and 4 to obtain 24-bit, 36-bit, and 48-bit codes, respectively. We adopt $D = 2048$ for 24-bit and 48-bit codes, while it is tweaked to 2049 for 36-bit codes. Note that we do not provide the 64-bit result for GPQ since 64-bit does not support a reasonably large value of K .

The comparison of mAP performance on VGGFace2 subset is shown in Table II. From Table II, it is clear that the proposed OPQN method outperforms all the compared methods over the entire code length range. Specifically, it surpasses the two strong competitors, i.e., DCDH [11] and DDQH [10], by 3.18% and 4.85% on average, respectively. Regarding the trade-off between performance and efficiency, the more than 95% mAP with just 36-bit codes is 4.09% higher than the second place DCDH. On the contrary, one can see a noticeable drop in the performance from OPQN to the variant method OPQN-l2q. Moreover, the performances of OPQN-l2q and DPQ are much poorer than their hashing-based counterparts DCDH and DDQH, especially under the code length of 24-bit. Once again, the results indicate that l2q-based methods,

which ignore the codewords’ inherent angular distribution, suffer from bad quantization quality when the original feature space is divided into only a few subspaces. Besides, the general task-oriented loss functions are insufficient to draw powerful feature representations or integrate all the visual information in each subspace for quantization.

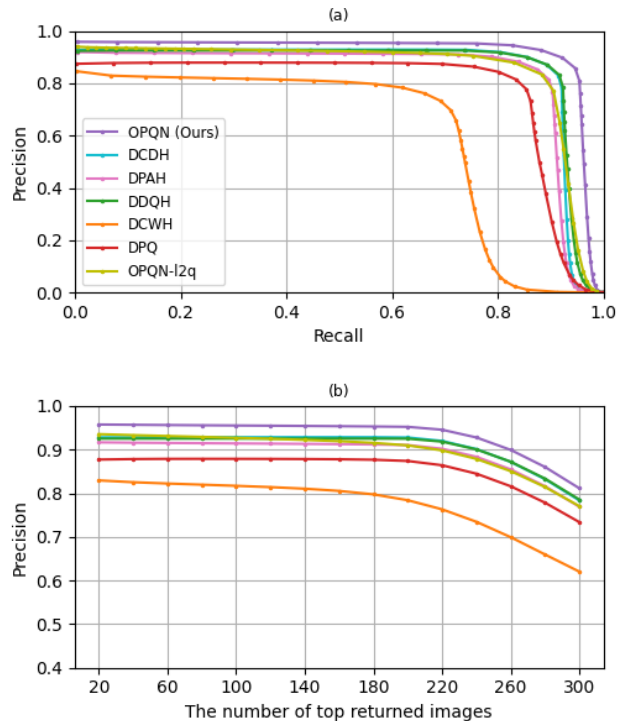


Fig. 6. (a) PR-curve performances under 64-bit codes on the subset of VGGFace2 dataset, (b) Precision w.r.t. different number of top returned images under 64-bit codes on the subset of VGGFace2 dataset.

We plot PR and $P@T$ curves under 64-bit codes by different methods in Fig. 6 (a) and Fig. 6 (b), respectively. It is clear that the proposed OPQN achieves the best performance of both PR-curve and $P@T$ compared to other methods. In combination with the previous results on FaceScrub and CFW-60K datasets, it shows that our method is robust to different evaluation metrics. As shown in Fig. 6 (b), we compute $P@T$ for up to 300 images in the database, which is the average number of images belonging to one identity. It is worth observing that our OPQN is the only method that maintains higher than 80% precision in the top 300 positions. Considering that the large pose and age variations in the VGGFace2 dataset, the capability of retrieving more than 80% of the related images is still encouraging.

Finally, to intuitively compare the feature representations learned in a subspace by different deep quantization methods, we illustrate visualizations of the sub-vector feature representations under 36-bit codes on the employed VGGFace2 dataset. We randomly select ten identities in the testing set, and deploy the trained deep quantization models on the samples to generate feature vectors directly. Note that instead of using the complete vector for visualization, it is more meaningful to visualize sub-vectors, for which the quantization is performed by each codebook individually. In our case, we split the first 512-dimensional features from 2048-dimensional bottleneck

features. t-SNE [33] is applied to map the high-dimensional features of each method to 2-dimensional. As we can see from Fig. 7, our proposed OPQN produces the most separable feature representations in the subspace with the least overlapping compared to other methods. The visualization results confirm that the proposed OPQN has the most discriminating power to learn sub-vectors of feature representations for quantization.

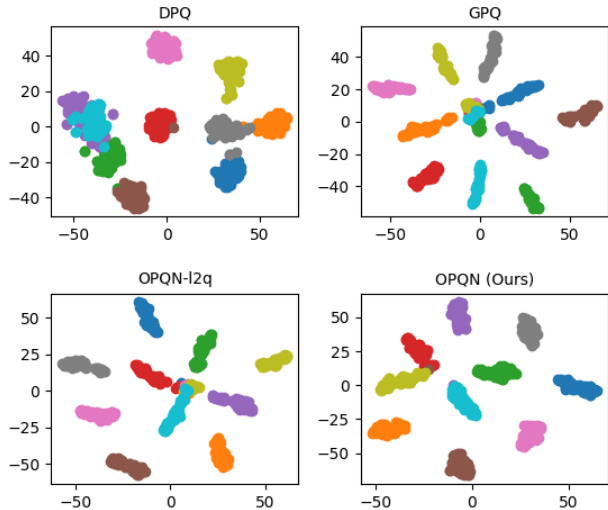


Fig. 7. Visualization of 10-class deep feature representations in a subspace produced by DPQ, GPQ, OPQN-l2q, and our proposed OPQN. Each color represents a unique identity.

As a summary of the three-dataset results under the single-domain setting, we owe the superiority of our method to the following two aspects. Firstly, by introducing the concepts of quantization to learning, the orthonormal codewords help enhance quantization informativeness and reduce the codewords redundancy. Besides, the applied soft quantization strategy explicitly disentangles the feature and probability, which provides much flexibility in quantization compositions when codewords are predefined. Secondly, benefiting from the joint subspace-wise classification loss, the network can not only maximize the discriminability in soft quantizations, but also in the original features, while the optimization on the latter facilitates the obtaining of better quantization representations in return. We illustrate the comparison of the PR curve w.r.t. other code lengths on FaceScrub, CFW-60K, and VGGFace2 datasets, in Figs. 8, 9, and 10, respectively.

E. Group 2: Cross-domain retrieval

In this section, we present the results under the setting of cross-domain retrieval. Unlike the single-domain retrieval, where the dataset for evaluation contains the same set of classes as in the training, we evaluate a set of unseen classes as queries and the database in cross-domain retrieval. The importance of cross-domain retrieval for examining a hashing technique has been highlighted in [14], whereas, we notice that none of the prior works of hashing-based face image retrieval has provided the results under this setting.

The employed protocol is given as follows. We apply all the deep hashing/quantization models pre-trained on the training

set of VGGFace2 subset as presented under single-domain retrieval. They are directly used for feature extraction and representation of images of unseen identities. We conduct evaluation on two different datasets. One is the official test set of VGGFace2, with its image items further divided into a database-query split as detailed in Section IV-A3. The second one is the CFW-60K dataset. We deploy the same training-testing split as in prior experiments regarding the database images and query items. Because of the specificity of face image retrieval tasks, users may lose interest in searching the lower-ranking results from a full list of returns if the top returned results have little relevance. Thus, we adopt $P@T$ as the evaluation metric instead of mAP to emphasize the top ranking rather than the overall ranking. Specifically, $P@10$ and $P@5$ are used for cross-domain retrieval on VGGFace and CFW-60K datasets, respectively.

The results of cross-domain retrieval on two datasets are shown in Table III. From Table III, it is obvious that all the pre-trained deep quantization/hashing models deteriorate much to unseen identities compared to their counterparts on single-domain retrieval. However, the pre-trained model by the proposed OPQN generalizes significantly better than other compared baselines. Specifically, it achieves the best 66.32% $P@10$ and 53.28% $P@5$ results on VGGFace2 and CFW-60K datasets, 25.75% and 24.84% higher than the second-place competitors DPQ and DDQH, respectively. And it boosts the cross-domain performance on VGGFace2 dataset by 23.34% and CFW-60K dataset by 20.92% on average. Once again, we see considerable improvements in performance by using the predefined orthonormal codewords in our method compared with OPQN-l2q.

There are two noteworthy observations from Table III. Firstly, the results of baseline deep quantization methods as well as our variant method are comparable or even better than the deep hashing methods, especially on smaller bits. However, these deep quantization methods perform inferior to their deep hashing competitors in the task of single-domain retrieval, as shown in Tables II and I. Therefore, it implies that the generalization ability of quantization-based methods is superior to hashing-based methods for face image retrieval. The reason is that unlike hashing methods which cause information loss from real-valued features to binary codes, PQ-based methods use real-valued codewords to alleviate the deviations generated during encoding. Besides, via the exponential number of combinations on codewords, they also enable more fine-grained and diverse distance measurements between the database and queries. The second observation from Table III is that the cross-domain retrieval performances exhibit a consistent and steady increase on $P@T$ with growth of the code lengths for all the methods. In contrast, the growth in model performances under single-domain retrieval slows down gradually with increased code length. For example, our method achieves slightly more than 95% performances with minor variations ranging from 36-bit to 64-bit. We conclude that longer binary code representations effectively improve the generalization ability of deep hashing/quantization methods. Last but not least, it is feasible for our method to learn longer than 64-bit codes by enlarging bottleneck features dimension

TABLE III
P@T RESULTS ON VGGFACE2 AND CFW-60K UNDER CROSS-DOMAIN SETTING

Method	VGGFace2 (P@10)				CFW-60K (P@5)			
	24-bit	36-bit	48-bit	64-bit	24-bit	36-bit	48-bit	64-bit
DDQH	0.1985	0.2728	0.3391	0.4000	0.1394	0.2014	0.2349	0.2844
DCWH	0.1367	0.2313	0.3058	0.3598	0.0846	0.1426	0.2024	0.2435
DPAH	0.1221	0.2161	0.2753	0.4038	0.0821	0.1429	0.1758	0.2673
DCDH	0.1426	0.2063	0.2915	0.3489	0.1003	0.1583	0.1828	0.2336
DPQ	0.2151	0.2621	0.3407	0.4057	0.1492	0.1768	0.1900	0.2677
GPQ	0.2051	0.2165	0.2258	-	0.1658	0.1682	0.1724	-
OPQN (Ours)	0.3987	0.5131	0.5823	0.6632	0.3050	0.4090	0.4500	0.5328
OPQN-12q	0.2638	0.3664	0.4788	0.5976	0.1894	0.2508	0.3691	0.4750

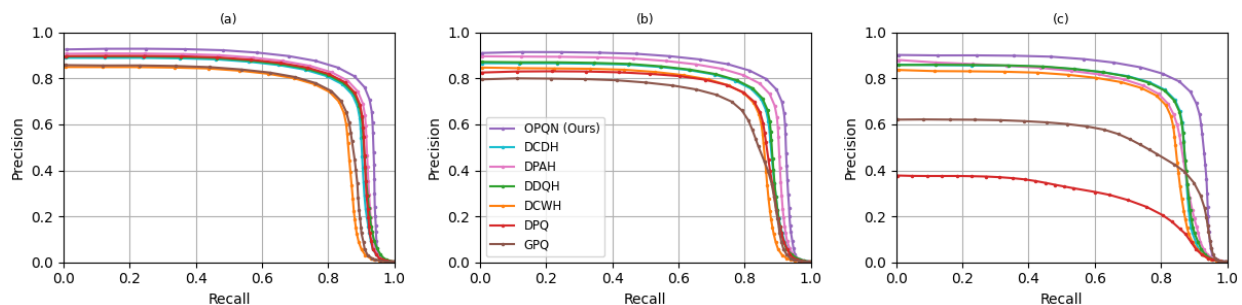


Fig. 8. Results of PR curve performance on FaceScrub dataset w.r.t different code lengths: (a) 36-bit, (b) 24-bit, (c) 16-bit.

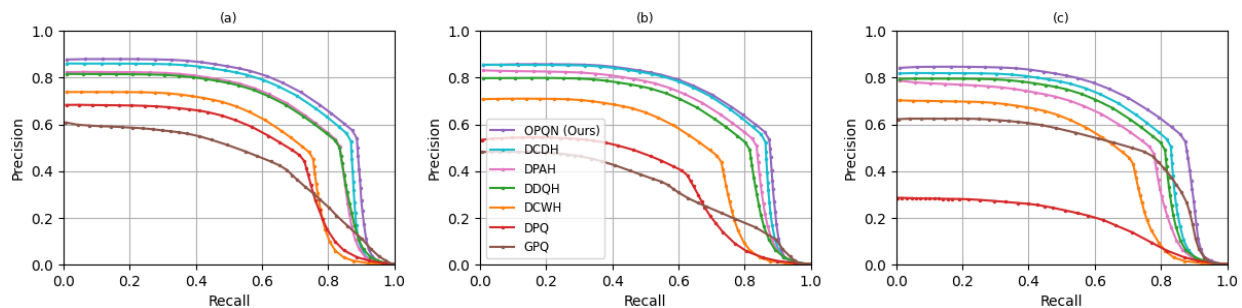


Fig. 9. Results of PR curve performance on CFW-60K dataset w.r.t different code lengths: (a) 36-bit, (b) 24-bit, (c) 16-bit.

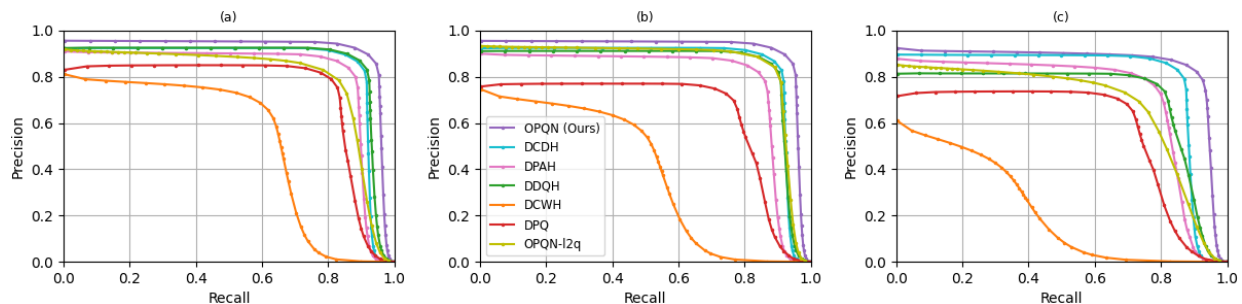


Fig. 10. Results of PR curve performance on VGGFace2 dataset w.r.t different code lengths: (a) 48-bit, (b) 36-bit, (c) 24-bit.

TABLE IV
MAP RESULTS OF THREE VARIANTS OF OUR METHOD FOR SINGLE-DOMAIN RETRIEVAL

Method	FaceScrub				CFW-60K			
	16-bit	24-bit	36-bit	48-bit	16-bit	24-bit	36-bit	48-bit
OPQN-A	0.6059	0.8762	0.8932	0.8989	0.2348	0.7497	0.8052	0.8172
OPQN-C	0.6164	0.8807	0.8390	0.8311	0.5455	0.7847	0.7384	0.7423
OPQN-S	0.2016	0.2892	0.6072	0.7888	0.1686	0.2618	0.6215	0.7281
OPQN-W	0.8066	0.9072	0.9240	0.9336	0.7338	0.8539	0.8789	0.8862
OPQN (Ours)	0.9032	0.9154	0.9270	0.9385	0.8547	0.8637	0.8826	0.8940

for better cross-domain retrieval performance.

V. DISCUSSION

A. Ablation study

To take a closer look at the proposed method with the carefully designed learning metric, we investigate four variant methods that apply different loss function design from our OPQN.

1) *OPQN-A*: In the OPQN-A method, the learning metric only utilizes the information within soft representations for training while the discriminability of original features is discarded. In other words, the classification loss L_{clf} in OPQN-A only contains the part derived in Eq. (7).

2) *OPQN-C*: The OPQN-C variant represents the strategy in which the composed soft representations and original sub-vectors in all the subspaces are concatenated to full vectors before being fed into the classifier. Specifically, OPQN-C considers ensemble x_i and s_i with the whole dimension, and the weight matrix of the classifier is also adjusted to the whole dimension. Thus, it only utilizes the visual information of x_i and s_i in the concatenated space.

3) *OPQN-S*: The OPQN-S variant simply replaces the angular margin-based classifier with the traditional softmax classifier as used in DPQ. Thus, no ℓ_2 normalization is applied to sub-vectors, soft representations, or weight vectors, while it still keeps the features of utilizing both soft quantization and original feature vectors in each subspace for training.

4) *OPQN-W*: The OPQN-W variant represents the finalized objective function without the regularization term L_{ent} shown in Eq. (9). This variant is set to observe to what extent the one-hot encoding of codewords assignment can improve the retrieval performance.

For a fair comparison, we apply the same codeword configuration as the original OPQN to four variants. Note that these variants all use predefined orthonormal codewords as ours. We report the mAP results of these variants on FaceScrub and CFW-60K datasets in Table IV. One can see that all these methods exhibit different degrees of performance deterioration compared to the proposed OPQN. The comparison of OPQN-A and our method proves that involving original feature information in training is beneficial to obtain more discriminative representations. We can also find a remarkable improvement in performance from OPQN-C to our method. It verifies the advantage of discriminability maximization in each subspace for better quantization precision. The OPQN-S performs the worst among the four variants. As our method

TABLE V
COMPARISON OF MAP RESULTS BY DIFFERENT CODEBOOK CONFIGURATIONS

Dataset	24-bit		36-bit		48-bit	
	4×6	3×8	6×6	4×9	8×6	6×8
FaceScrub	0.9154	0.9298	0.9270	0.9367	0.9385	0.9329
VGGFace2	0.7722	0.8986	0.9026	0.9508	0.9386	0.9504

works with sub-vectors instead of concatenated full vectors as in DPQ, it indicates the necessities of ℓ_2 normalization and angular margin for radius variations removal and separable representations learning in our case. Finally, from the comparison of OPQN-W and our method, we find the entropy-based regularization boosts the performance under tiny code lengths, e.g., 16-bit, while for longer bits, our OPQN slightly performs better than OPQN-W. Basically, the one-hot encoding prompts smaller quantization errors to use hard quantization to represent database items. The reason could be that the disturbance from quantization error is much more severe under tiny bits, whereas the adverse impact is lessened with more possible combinations of codewords in longer bits.

B. Codebook configuration

We further explore the influence of different codebook configurations on binary code performances. Basically, a l -bit binary code can be generated in the form of $l = M \times O$, where M is the number of codebooks, $O = \log_2 K$, and K is the number of codewords per codebook. Thus, the binary codes with the same length can be obtained from different combinations of M and O . For simplicity, we consider two relative configurations with a general K ranging between 2^6 and 2^9 : the first configuration adopts bigger M and smaller O for encoding while the other uses smaller M and bigger O instead. We conduct two sets of experiments on 24-bit, 36-bit, and 48-bit codes, w.r.t two configurations, respectively. The combinations of the first configuration are 4×6 , 6×6 , and 8×6 for three code lengths, respectively, while the other configuration uses 3×8 , 4×9 , 6×8 under three code lengths respectively. The results on FaceScrub and VGGFace2 under the single-domain setting are presented in Table V.

From Table V, we can see a certain degree of performance improvement under almost all the cases when using a larger O for quantization. And the improvements are more distinct for the VGGFace2 dataset than for FaceScrub. We can conclude that our method prefers to work with a larger value of K

TABLE VI
16-BIT MAP RESULTS W.R.T. DIFFERENT VALUES OF λ

λ	0	0.01	0.05	0.1	0.3
FaceScrub	0.8066	0.8247	0.8543	0.9032	0.0159
CFW-60K	0.7338	0.7628	0.7801	0.8547	0.1029

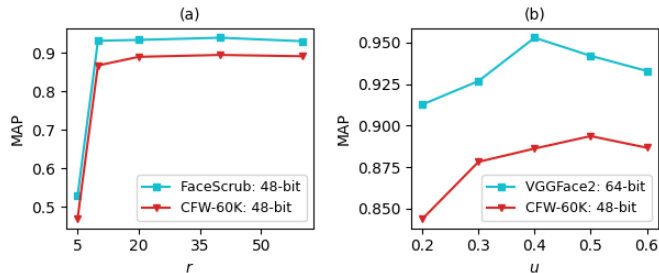


Fig. 11. (a) mAP results w.r.t. different values of the scaling factor r under the two experiment settings, (b) mAP results w.r.t. different values of the margin u under the two experiment settings.

especially for smaller bits. Intuitively, using more codewords in a codebook represents richer prototypes in the subspace for quantization. Thus, it is easier for sub-vectors to find the nearest prototype with less quantization error. One can see that by using $K = 256$ rather than $K = 64$ under 24-bit on VGGFace2 dataset, our method can easily reach nearly a 90% mAP score. And the performance of 36-bit codes with 4×9 configuration is even better than 48-bit codes. However, the benefit from larger K may become less impressive with longer bits. The reason is that the increase in the number of subspaces also helps to reduce the quantization burden, which can mitigate the requirement for a large value of K .

C. Parameter Sensitivity

Finally, we investigate the effect of parameters on the model performances. We first look at the balance weight λ . As we observe in the ablation study, the entropy-based regularization mainly exhibits its advantage under short codes. Thus, we present the mAP results w.r.t. different values of λ under 16-bit codes in Table VI. One can see that the performances steadily grows by adding the regularization with λ varying from 0.01 to 0.1. However, λ cannot be set to larger than 0.1 from the drastic drops on mAP observed in Table VI.

We then study the impacts of another two parameters: the scaling factor r and the angular margin u , as shown in Eq. (6) and Eq. (7). The plots of mAP performances w.r.t. different values of r and u are illustrated in Figs. 11(a) and 11(b), respectively. From Fig. 11(a), we can observe a substantial boost of the mAP from $r = 5$ to $r = 10$. With the further increase of r , the performances are slightly improved. In summary, the model performs well with r ranging from 20 to 50, and the performances stop growing when using larger values. Fig. 11 (b) shows that with an increase of u from 0.2 to 0.6, the model performance tends to rise at first then goes down gradually. The turning point on the VGGFace2 dataset appears ahead of the CFW-60K dataset. And the best value of u is around 0.4 in VGGFace2 while 0.5 in CFW-60K dataset.

Different from the tiny value of r leading to abysmal results, the model performs more robustly under variations of u .

VI. CONCLUSION

This paper developed a deep product quantization-based method for face image retrieval. Unlike previous deep quantization works, this paper proposed a novel framework using predefined orthonormal codewords for quantization. Furthermore, we designed a tailed loss function as the learning metric, which maximizes the discriminability in both soft quantizations and original features in all the subspaces. Extensive experiments were conducted on three widely-employed datasets in comparison with several deep hashing/quantization baselines. The results showed that the proposed method outperformed other compared methods under both single-domain and cross-domain settings. Meanwhile, other deep quantization methods can obtain competitive generalization performances compared with their deep hashing competitors even if their results for single-domain retrieval are inferior. Therefore, it verifies the inherent advantage of product quantization over binary hashing for cross-domain retrieval.

For future work, it is worth investigating how the complete visual information are scattered into subspaces in the quantization method. Specifically, the sub-vector of bottleneck features in different subspaces may describe specific facial region or attributes. Thus, our designed subspace-wise learning metric should also be adaptive to different parts of visual discriminability. This enables us to automatically choose optimal values of the margin u and the scaling factor r in our case.

ACKNOWLEDGMENT

This work is supported by the Hong Kong Innovation and Technology Commission and City University of Hong Kong (Project 9610460).

REFERENCES

- [1] B. Klein and L. Wolf, "End-to-end supervised product quantization for image search and retrieval," in *Proceedings of the IEEE Conference on Computer Vision and Pattern Recognition*, 2019, pp. 5041–5050.
- [2] Y. K. Jang and N. I. Cho, "Generalized product quantization network for semi-supervised image retrieval," in *Proceedings of the IEEE/CVF Conference on Computer Vision and Pattern Recognition*, 2020, pp. 3420–3429.
- [3] W.-J. Li, S. Wang, and W.-C. Kang, "Feature learning based deep supervised hashing with pairwise labels," in *IJCAI*, 2016, pp. 1711–1717.
- [4] Q. Li, Z. Sun, R. He, and T. Tan, "Deep supervised discrete hashing," in *NIPS*, 2017, pp. 2482–2491.
- [5] X. Wang, Y. Shi, and K. M. Kitani, "Deep supervised hashing with triplet labels," in *ACCV*. Springer, 2016, pp. 70–84.
- [6] X. Zhe, S. Chen, and H. Yan, "Deep class-wise hashing: Semantics-preserving hashing via class-wise loss," *IEEE transactions on neural networks and learning systems*, vol. 31, no. 5, pp. 1681–1695, 2020.
- [7] L. Yuan, T. Wang, X. Zhang, F. E. Tay, Z. Jie, W. Liu, and J. Feng, "Central similarity quantization for efficient image and video retrieval," in *CVPR*, 2020, pp. 3083–3092.
- [8] M. Zhang and H. Yan, "Improved deep classwise hashing with centers similarity learning for image retrieval," in *2020 25th International Conference on Pattern Recognition (ICPR)*. IEEE, 2021, pp. 10516–10523.
- [9] J. Lin, Z. Li, and J. Tang, "Discriminative deep hashing for scalable face image retrieval," in *IJCAI*, 2017, pp. 2266–2272.

- [10] J. Tang, J. Lin, Z. Li, and J. Yang, "Discriminative deep quantization hashing for face image retrieval," *IEEE transactions on neural networks and learning systems*, vol. 29, no. 12, pp. 6154–6162, 2018.
- [11] M. Zhang, X. Zhe, S. Chen, and H. Yan, "Deep center-based dual-constrained hashing for discriminative face image retrieval," *Pattern Recognition*, p. 107976, 2021.
- [12] H. Jegou, M. Douze, and C. Schmid, "Product quantization for nearest neighbor search," *IEEE transactions on pattern analysis and machine intelligence*, vol. 33, no. 1, pp. 117–128, 2010.
- [13] Y. Cao, M. Long, J. Wang, H. Zhu, and Q. Wen, "Deep quantization network for efficient image retrieval," in *Proceedings of the AAAI Conference on Artificial Intelligence*, vol. 30, no. 1, 2016.
- [14] A. Sablayrolles, M. Douze, N. Usunier, and H. Jégou, "How should we evaluate supervised hashing?" in *2017 IEEE International Conference on Acoustics, Speech and Signal Processing (ICASSP)*. IEEE, 2017, pp. 1732–1736.
- [15] H.-W. Ng and S. Winkler, "A data-driven approach to cleaning large face datasets," in *ICIP*. IEEE, 2014, pp. 343–347.
- [16] Y. Li, R. Wang, H. Liu, H. Jiang, S. Shan, and X. Chen, "Two birds, one stone: Jointly learning binary code for large-scale face image retrieval and attributes prediction," in *ICCV*, 2015, pp. 3819–3827.
- [17] Q. Cao, L. Shen, W. Xie, O. M. Parkhi, and A. Zisserman, "Vggface2: A dataset for recognising faces across pose and age," in *FG*. IEEE, 2018, pp. 67–74.
- [18] Y. K. Jang, D.-j. Jeong, S. H. Lee, and N. I. Cho, "Deep clustering and block hashing network for face image retrieval," in *Asian Conference on Computer Vision*. Springer, 2018, pp. 325–339.
- [19] Z. Xiong, D. Wu, W. Gu, H. Zhang, B. Li, and W. Wang, "Deep discrete attention guided hashing for face image retrieval," in *Proceedings of the 2020 International Conference on Multimedia Retrieval*, 2020, pp. 136–144.
- [20] A. Babenko and V. Lempitsky, "Additive quantization for extreme vector compression," in *Proceedings of the IEEE Conference on Computer Vision and Pattern Recognition*, 2014, pp. 931–938.
- [21] T. Zhang, C. Du, and J. Wang, "Composite quantization for approximate nearest neighbor search," in *International Conference on Machine Learning*. PMLR, 2014, pp. 838–846.
- [22] B. Liu, Y. Cao, M. Long, J. Wang, and J. Wang, "Deep triplet quantization," in *Proceedings of the 26th ACM international conference on Multimedia*, 2018, pp. 755–763.
- [23] T. Yu, J. Yuan, C. Fang, and H. Jin, "Product quantization network for fast image retrieval," in *Proceedings of the European Conference on Computer Vision (ECCV)*, 2018, pp. 186–201.
- [24] N. Ahmed, T. Natarajan, and K. R. Rao, "Discrete cosine transform," *IEEE transactions on Computers*, vol. 100, no. 1, pp. 90–93, 1974.
- [25] H. Wang, Y. Wang, Z. Zhou, X. Ji, D. Gong, J. Zhou, Z. Li, and W. Liu, "Cosface: Large margin cosine loss for deep face recognition," in *Proceedings of the IEEE Conference on Computer Vision and Pattern Recognition*, 2018, pp. 5265–5274.
- [26] J. Deng, J. Guo, N. Xue, and S. Zafeiriou, "Arcface: Additive angular margin loss for deep face recognition," in *Proceedings of the IEEE Conference on Computer Vision and Pattern Recognition*, 2019, pp. 4690–4699.
- [27] K. Zhang, Z. Zhang, Z. Li, and Y. Qiao, "Joint face detection and alignment using multitask cascaded convolutional networks," *IEEE Signal Processing Letters*, vol. 23, no. 10, pp. 1499–1503, 2016.
- [28] R. Wang, R. Wang, S. Qiao, S. Shan, and X. Chen, "Deep position-aware hashing for semantic continuous image retrieval," in *Proceedings of the IEEE/CVF Winter Conference on Applications of Computer Vision*, 2020, pp. 2493–2502.
- [29] K. He, X. Zhang, S. Ren, and J. Sun, "Deep residual learning for image recognition," in *Proceedings of the IEEE conference on computer vision and pattern recognition*, 2016, pp. 770–778.
- [30] W. Liu, Y. Wen, Z. Yu, M. Li, B. Raj, and L. Song, "Spheroface: Deep hypersphere embedding for face recognition," in *Proceedings of the IEEE conference on computer vision and pattern recognition*, 2017, pp. 212–220.
- [31] N. Srivastava, G. Hinton, A. Krizhevsky, I. Sutskever, and R. Salakhutdinov, "Dropout: a simple way to prevent neural networks from overfitting," *Journal of Machine Learning Research*, vol. 15, no. 1, pp. 1929–1958, 2014.
- [32] S. Ioffe and C. Szegedy, "Batch normalization: accelerating deep network training by reducing internal covariate shift," in *International Conference on Machine Learning (ICML)*, 2015, pp. 448–456.
- [33] L. v. d. Maaten and G. Hinton, "Visualizing data using t-sne," *Journal of machine learning research*, vol. 9, no. Nov, pp. 2579–2605, 2008.